Coarse-Grid and Cloud-Resolving Simulations of a Midlatitude Cyclonic Cloud System: Implications for the Parameterization of Layer Clouds in GCMs

K. K. SZETO AND H. GUAN

Atmospheric Environment Service, Downsview, Ontario, Canada

27 May 1999 and 9 November 1999

ABSTRACT

A winter oceanic cyclonic cloud system was simulated by using the mesoscale compressible community (MC2) model with different combinations of model resolutions and cloud microphysics packages. Results from these simulations are intercompared to examine the effects of the coarse model grid and simplified model physics on the simulated large-scale storm environment. When aggregated to an area approximately equivalent to the size of a grid box in current GCMs, the results from the models differ significantly in the large-scale cloud and moisture profiles. Although the effects of using different stratiform cloud schemes on the coarse-grid results are appreciable, the effects of different model resolution are shown to be greater on the large-scale frontal cloud field. In particular, the coarse-grid models underestimated the cloudiness and atmospheric moisture content in the warm-frontal region. Such differences in the large-scale model storm environment were consequences of the stronger mean cross-front circulation and mesoscale cloud features in the high-resolution simulation. The stronger cross-front circulation was in turn a result of stronger frontogenetic processes over the region and dynamic influences of the mesoscale cloud bands on the parent storm. Because both the frontal zones and the mesoscale cloud bands are unresolved features in current GCMs, these results suggest that the parameterization of their bulk effects on the large scales should be included in the representation of frontal layered clouds in climate models.

1. Introduction

It is generally agreed that cloud effects are responsible for some of the most fundamental uncertainties in current climate models and that the improvement of their representation in coupled ocean–atmospheric general circulation models (GCMs) should be among the top priorities in future climate model developments (Houghton et al. 1996). Although atmospheric convection is the main cloud- and precipitation-producing mechanism in the Tropics, cyclonic systems are responsible for much of the clouds and precipitation in extratropical regions. The cloud structures associated with these synoptic systems are extensive, complex, and typically comprise a rich mixture of interacting convective, layered, and stratiform components (Stewart et al. 1998). This latter aspect makes the parameterization of the cloud effects of these systems in climate models a challenging and difficult problem. Collectively, these midlatitude synoptic-scale cloud systems can significantly modify the large-scale tropospheric and surface environments. For example, the underprediction of moisture content in the upper troposphere and the overprediction of solar absorption at the surface over the storm-track regions are common deficiencies in current climate simulations. The underestimate of synoptic clouds over the storm tracks is believed to be at least partially responsible for these model deficiencies (Del Genio 1996; Stewart et al. 1998). Furthermore, analysis of snapshots of the model outputs suggests that clouds were particularly underestimated near the frontal zones (Del Genio 1996).

Because synoptic systems cover an extensive area and observations representative of an area comparable to a GCM grid square are not typically available, direct validation of GCM simulations of a particular system is not usually a feasible task. Instead, high-resolution cloud-resolving model (CRM) simulations of observed cloud systems can be more readily validated with local conventional ground-based and airborne observations. Once validated, the CRM results can be compared with coarse-grid simulation results to assess the capability of the coarse-grid model in simulating the large-scale cloud effects of these systems. In this paper, results from CRM and coarse-grid simulations of a typical oceanic winter cyclone that occurred over the western flank of the North Atlantic storm track will be compared to examine the effects of coarse model resolution and different cloud microphysics on the large-scale thermal and kinematic conditions of the storm. The implications of the results

Corresponding author address: Kit K. Szeto, CCRP, AES, 4905 Dufferin Street, Downsview, ON M3H 5T4, Canada.
E-mail: kit.szeto@ec.gc.ca

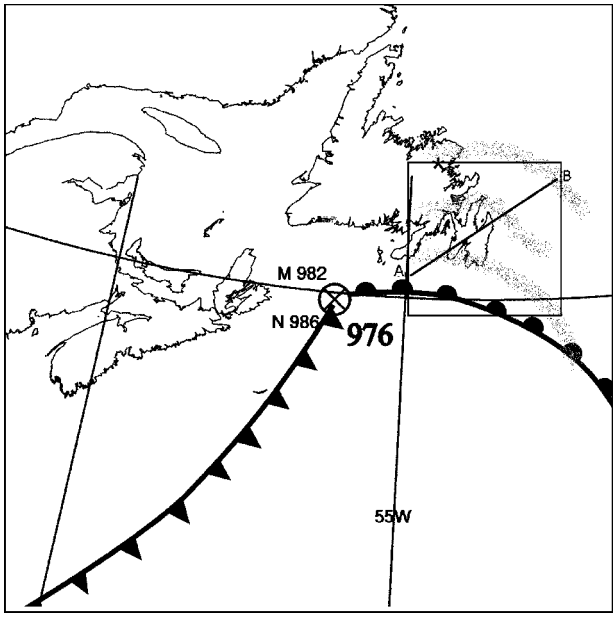

FIG. 1. Synoptic conditions near Newfoundland, Canada, at 0000 UTC 27 Feb 1992. Also shown in the figure are the observed (×) and simulated (M for HR10 and N for CG150-S) low pressure centers (mb), locations of the three observed precipitation bands, and the 300 km × 300 km box A for the intercomparison of the model results, as well as the location of the cross section AB for Figs. 2 and 3. The low center for CG150-KY is located near N but with a center pressure of 988 mb instead.

for future improvements of GCM cloud parameterizations will also be discussed.

2. Case study and simulations

The test case was a typical winter cyclone deepening rapidly off the east coast of North America on 26–27 February 1992. A detailed observational analysis of the case is given in Hudak et al. (1996); only a brief summary of the observed system will be presented here. The warm front associated with this system approached the southern coast of Newfoundland, Canada, at around 0000 UTC 27 February. Virtually all of the precipitation was ahead of the warm front. The main precipitation area, which passed over eastern Newfoundland between about 2000 UTC 26 February and 0000 UTC 27 February, was in the form of three banded structures oriented parallel to the warm front (Fig. 1). After 0000 UTC 27 February the occlusion process began as the low tracked across central Newfoundland. Surface precipitation changed from snow in the band located farthest ahead of the surface front to mixed snow/rain in the second band and rain in the band closest to the front. Frontal uplift, weak convection, and conditional symmetric instability had been diagnosed to be responsible for the formation of these bands. Mixed-phase cloud microphysical processes are also found to be important in the dynamics of these mesoscale storm features (Hudak et al. 1996; Szeto et al. 1999).

The model used in this study is the fully compressible, semi-implicit, semi-Lagrangian, three-dimensional, nonhydrostatic mesoscale compressible community (MC2) model (Benoit et al. 1997). Some characteristics of the model include variable vertical resolution, modified Gal-Chen terrain-following vertical coordinate, limited-area one-way nesting capability, a complete physics package including several cloud schemes of various degrees of sophistication, and a turbulence kinetic energy boundary layer parameterization scheme. Canadian Meteorological Centre analyses were used to provide the initial and boundary conditions for the simulations. A high-resolution simulation (HR10, 10-km horizontal resolution one-way nested within 25- and 50-km resolution domains) of the system was performed with the Kong-Yau cloud microphysical scheme (Kong and Yau 1997), which includes five categories of water substances (water vapor, cloud water, rain, ice–snows, and graupel). Two parallel coarse-grid (150-km resolution) simulations (CG150-KY and CG150-S) were also performed. The (unmodified) Kong–Yau cloud scheme was used in the CG150-KY simulation. The CG150-S simulation was performed with the Sundqvist cloud scheme (Sundqvist et al. 1989), which is commonly used in current GCMs. Thirty-three vertical levels with a model lid at 18 km were used in all simulations. The vertical grid size was constant at 250 m in the lowest 5 km and increasing to about 2000 m near the top of the domain.

Results from these simulations will be compared to examine the effects of coarse spatial resolution and simplified cloud microphysics on the large-scale structure of the mature cloud system. The intercomparisons will be focused on the mature warm-frontal region where the most significant cloud and precipitation features were found in this system (Hudak et al. 1996). The effects of the storm on the large-scale state of the atmosphere will be examined by spatially averaging the model variables over a 300 km × 300 km (typical size of a grid box in current GCMs for long-term simulations) square (A) located over eastern Newfoundland (Fig. 1).

3. Results and discussions

Details of the HR10 simulation as well as its validation against observations can be found in Szeto et al. (1999). In this article, we will concentrate on the intercomparison of results from HR10 and the coarse-grid simulations; only a brief summary of the validation of HR10 with observations will be presented. Both the evolution of the low pressure system (see Fig. 1 and Szeto et al. 1999) as well as the associated cloud and precipitation features were reasonably well simulated in HR10. In particular, the observed warm-frontal structure (e.g., the temperature field and low-level jet structures) and the three observed warm-frontal precipitation bands were replicated quite well in the simulation (Figs. 2a,b).

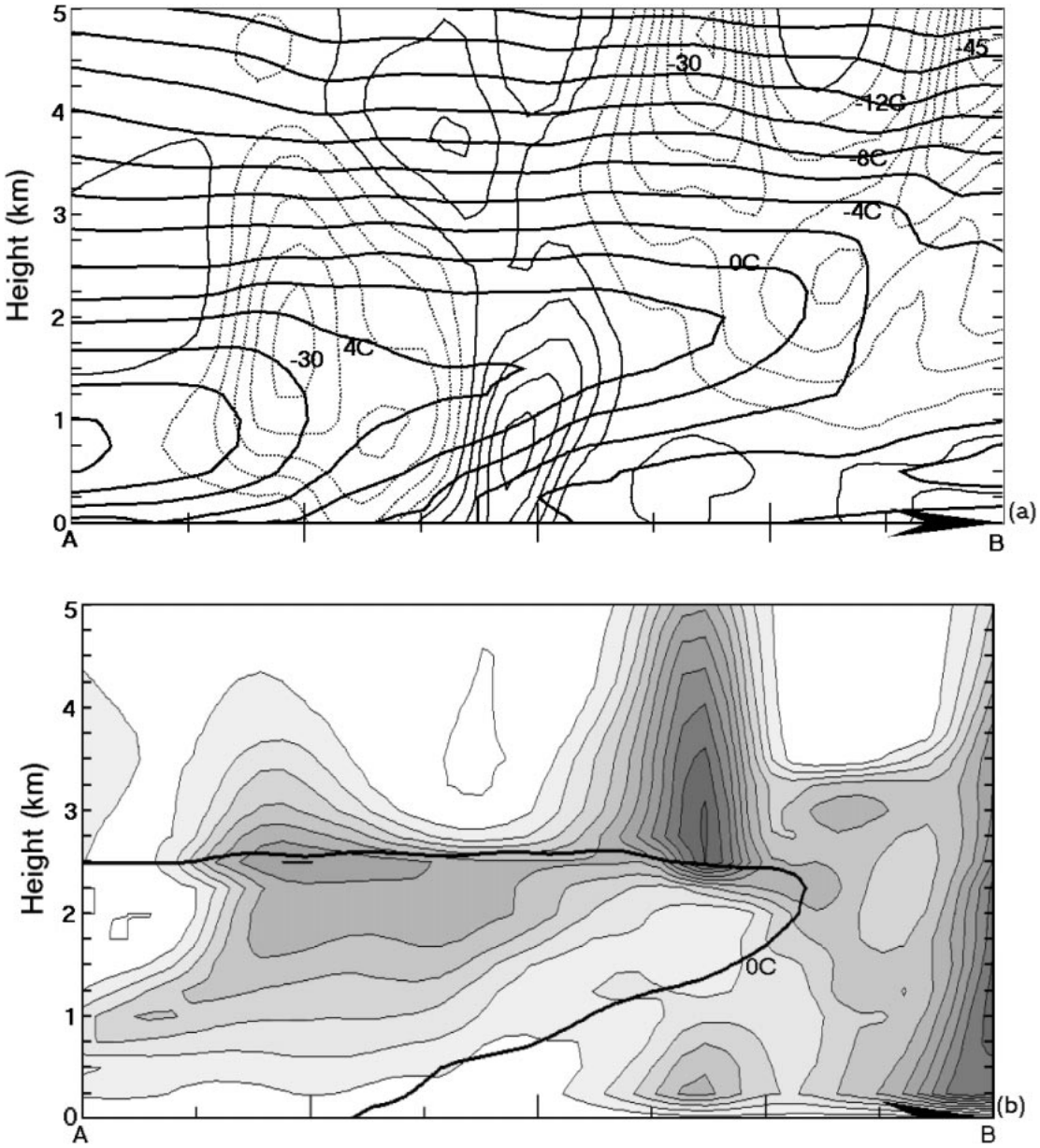

FIG. 2. Horizontal cross sections of (a) temperature (2 K intervals) and pressure velocity (5 Pa s^{-1} intervals), and (b) total (liquid + ice) cloud mixing ratio (0.1 g kg^{-1} shading intervals) for HR10 at 0000 UTC 27 Feb.

The complex mesoscale cloud and precipitation structures associated with this kind of system are evident in Fig. 2b and these features are unresolved in current GCMs as well as in the present coarse-grid simulations.

In comparison, the model storm is not as well developed in CG150-KY and CG150-S. While the tracks of the low pressure center are similar among the observations, HR10, and the coarse-grid simulations, the center pressure was consistently higher in the coarse-grid simulatoins (Fig. 1). Although the overall N–S temperature gradients over box A at 0000 UTC 27 February was about 3 K $(100\ km)^{-1}$ for all three model systems, the strongest warm-frontal horizontal temperature contrast was about 6.5 K $(100\ km)^{-1}$ in HR10, while it was only about 3.5 K $(100\ km)^{-1}$ in CG150-KY and CG150-S. The mean precipitation rate over A is ~2.3 mm h^{-1} for CG150-S, ~2.1 mm h^{-1} for CG150-KY, and ~3 mm h^{-1} for HR10.

The vertical cross sections of temperature and cloud mixing ratio along line AB for case CG150-S are given in Fig. 3. Despite the coarse horizontal resolution used in CG150-S, the gross thermal structures (e.g., the enhanced horizontal temperature gradient in the ''frontal zone'' and the frontal inversion) were captured reason-

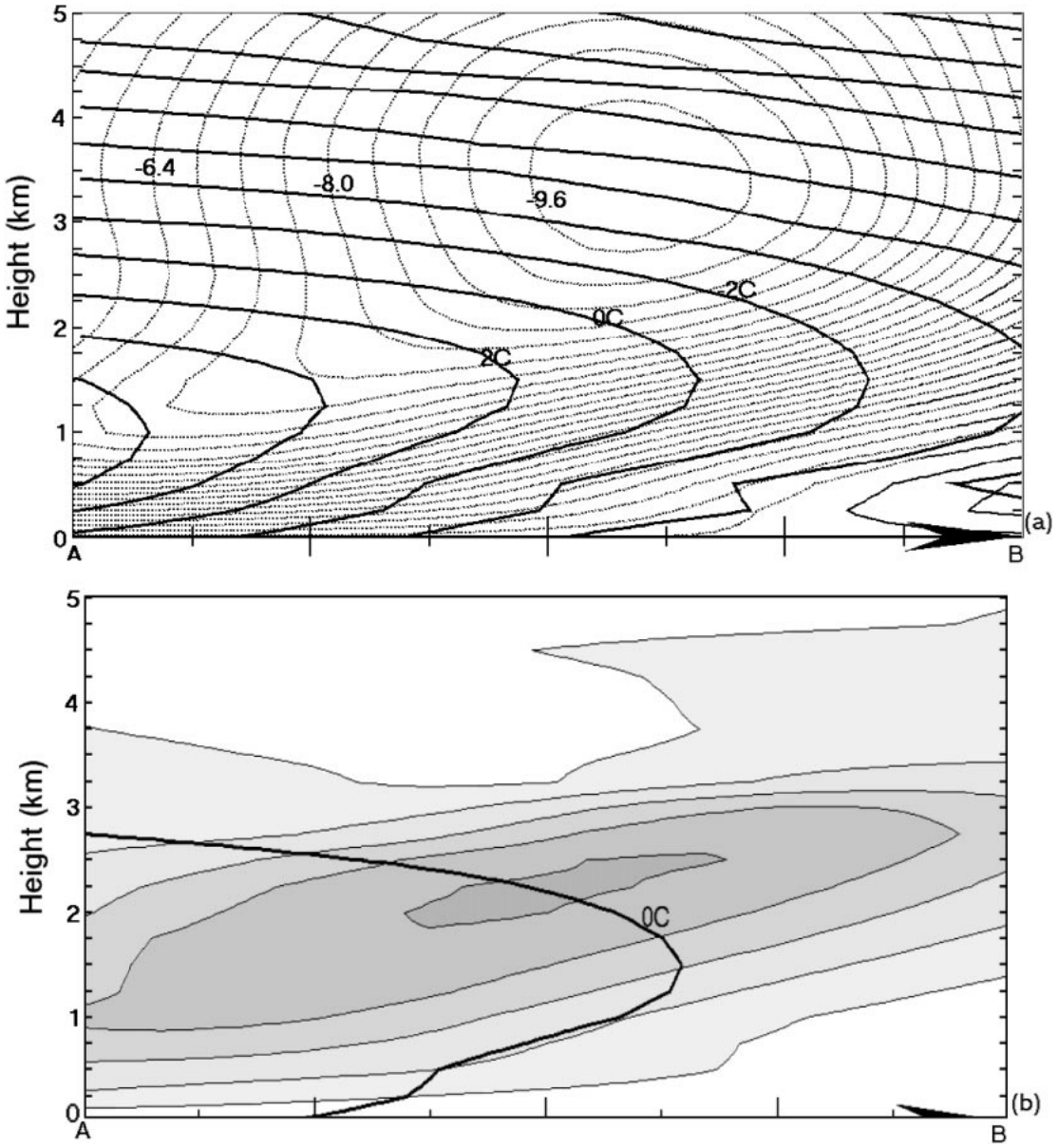

FIG. 3. As in Fig. 2 but for CG150-S.

ably well in the simulation. There was widespread weak updraft with a maximum updraft core (vertical velocity $\sim$ 15 cm s^{-1}) above the frontal zone at $\sim$4.5-km altitude. Cloud water was formed in response to this widespread vertical motion. The cloud layer was shallow ($\sim$2 km deep) and most of the cloud water was formed above the sloping frontal zone. The warm-frontal cloud and vertical motion fields in CG150-S are thus quite similar to those conceptualized in the classical polar front model (stratiform type cloud produced by a gentle upglide motion along the frontal surface). The storm structure in CG150-KY (not shown) was in general quite similar to that in CG150-S but with a slightly weaker vertical circulation and associated cloud field. Comparatively and expectedly, the frontal thermal and cloud structures in HR10 were more complicated and more similar to those revealed in modern observations (e.g., see Houze and Hobbs 1982). In particular, there were mesoscale features (warm-frontal bands) embedded within the general frontal upglide. Magnitudes of the vertical velocity, the cloud-top height, cloud mixing ratios, and precipitation rates associated with these bands are generally much higher than the average over box A. We will examine the effects of these mesoscale features on the large-scale thermal and kinematic environments over a region representative of a GCM grid box.

The horizontal averages of temperature (T), total cloud mixing ratio (q_c), along-front (W–E) wind (u),

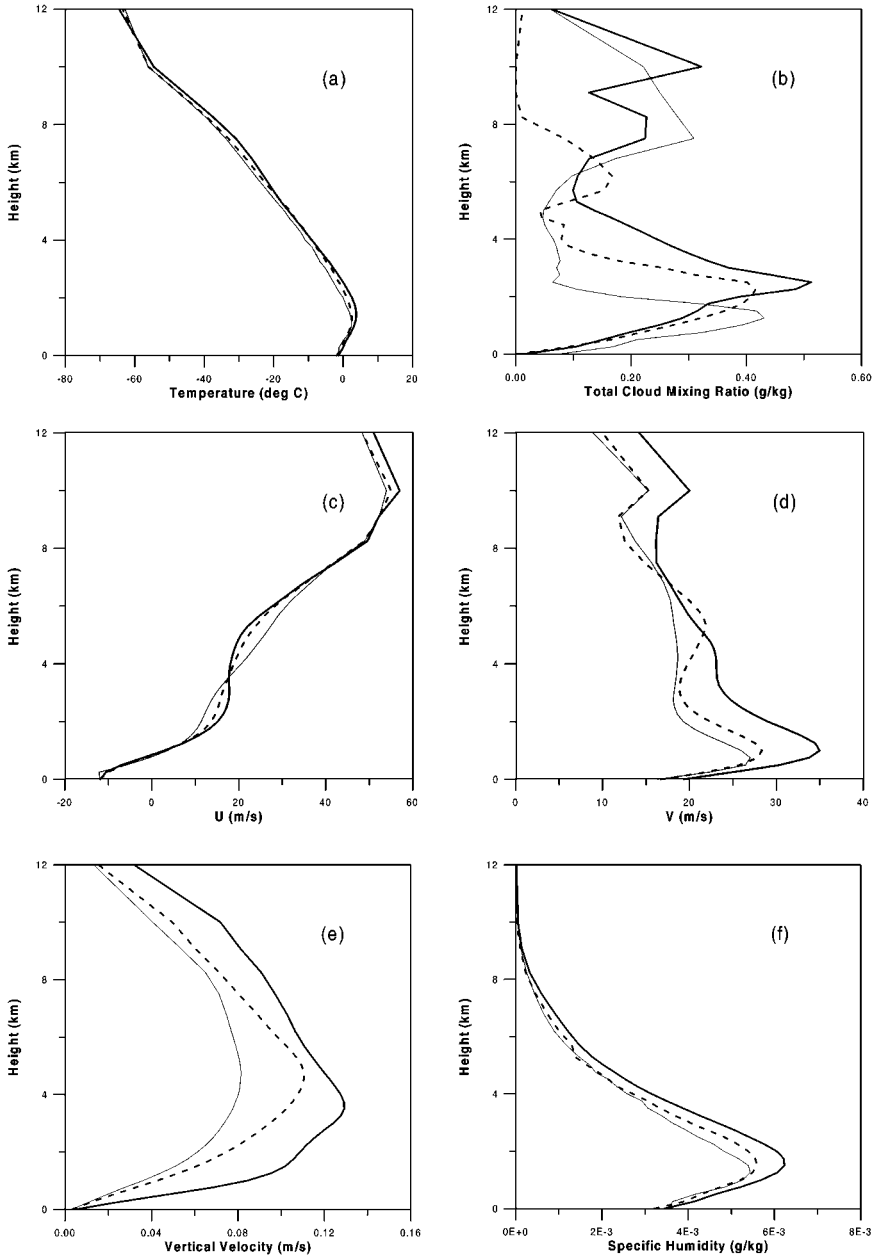

FIG. 4. Vertical profiles of horizontally averaged (a) temperature, (b) total (liquid + ice) cloud mixing ratio, (c) E–W velocity, (d) S–N velocity, (e) vertical velocity, and (f) specific humidity over box A at 0000 27 Feb for HR10 (thick line), CG150-S (dashed), and CG150-KY (thin line).

cross-front (S–N) wind (v), vertical velocity (w), and specific humidity (q) over box A for the simulations are presented in Fig. 4. The spatially averaged T profiles are very similar for all three simulations (Fig. 4a), suggesting that we are examining similar storm regions of the model systems. Tropospheric temperatures in CG150-KY are slightly lower than those in CG150-S and HR10, reflecting the weaker cloud field and associated latent heating in the former case (Fig. 4b). The slightly stronger inversion in HR10 was a result of the enhanced midlevel warm air advection by the stronger cross-front velocities in that case (Fig. 4d).

In agreement with the cross sections in Figs. 2 and 3, the HR10 storm possessed a deeper and stronger mean cloud structure than the coarse-grid cases (Fig. 4b). Since the Kong–Yau scheme was designed and calibrated for use with mesoscale and cloud-scale models, it is not too surprising that the mean cloud field was weakest in CG150-KY. In particular, the low- and midlevel frontal cloud deck was much shallower than those

in the HR10 and CG150-S cases. However, the upper-level cirrus structure in CG150-KY was more similar to that in HR-10 than in CG150-S, presumably due to the inclusion of the ice phase in the Kong–Yau scheme but not in the Sundqvist scheme. Since the large-scale vertical cloud structure are substantially different among the cases, the large-scale cloud radiational effects (not shown) should be quite different as well.

The along-front velocities (Fig. 4c) were very similar among the three cases. The similarity of the u profiles among the cases is a consequence of (i) the quasi-thermal wind balance of large-scale atmosphere and (ii) the similar net N–S temperature gradients across box A for the cases. On the other hand, both the averaged cross-front velocities (Fig. 4d) and vertical velocities (Fig. 4e) were significantly stronger in case HR10. These differences reflect the much stronger cross-front circulation in the HR10 case. This stronger cross-front circulation was a consequence of the stronger frontogenesis and dynamic influences of the mesoscale frontal cloud features on the model storm in the HR10 model storm (see Szeto et al. 1999 for detailed discussions on the frontal-scale dynamics of this case). As shown earlier, the stronger cross-front circulation in the HR10 storm contributed to the slightly warmer large-scale storm environment and deeper and denser clouds in the HR10 case. Although the mean cloud profiles at low levels are more similar between the HR10 and CG150-S cases, the low-level (<3-km altitude, where the frontal circulation is strongest) v and w profiles are more similar between the coarse-grid cases (Figs. 4d and 4e), suggesting that the unresolved dynamics could have more profound effects on the large-scale vertical circulation than the latent heating effects in this case.

The vertical profiles of mean specific humidity for the cases are shown in Fig. 4f. It is evident that the large-scale storm environment became significantly moister in HR10 as the storms evolved. The moister storm environment in the high-resolution case was partly a result of the stronger mean cross-front circulation that brought the boundary layer moisture to the higher levels. The vertical transports by frontal and mesoscale features also played an important role in this case. To examine the effects of the frontal and mesoscale features on the large-scale moisture field over A at 0000 UTC 27 February, the main terms contributing to the apparent moisture sink ($Q2$) are computed over a corresponding box for the HR10 system at 2100 UTC 26 February (Fig. 5). The apparent moisture sink is defined by

$$Q2 = -\frac{L}{C_p}\frac{\overline{Dq}}{Dt} = \frac{L}{\rho C_p}\frac{\partial}{\partial z}\overline{\rho w'' q''} + \dot{Q}_v + D_{Q2}, \quad (1)$$

where C_p is heat capacity of dry air, L is latent heat of vaporization, Q_v is heating rate associated with the phase change of water vapor only, ρ is air density, and D_{Q2} denotes subgrid-scale diffusions. The overbar denotes areal averaging over the box and the double primes

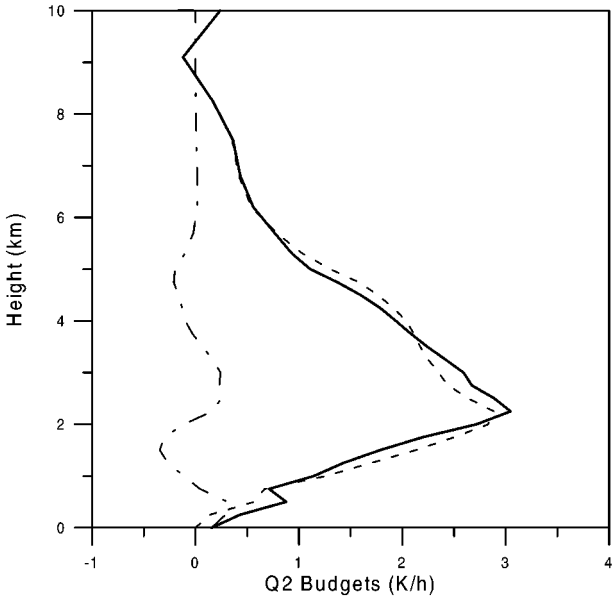

FIG. 5. Vertical profiles of $Q2$ budgets for the system in HR10 at 2100 UTC 26 Feb: (i) the latent heating (dashed line), (ii) the eddy (dashed-dotted), and (iii) the net (thick line) terms.

denotes deviations from the mean variables. The first term on the right side of Eq. (1) gives the mean vertical eddy moisture flux divergence associated with the cloud and mesoscale motions. The moistening effects (i.e., negative contributions to $Q2$) of these finescale features are evident between 0.8- and 2.1-km and between 3.7- and 5.7-km altitudes. The low-level moistening effects were due to the narrow low-level frontal updraft near the surface frontal zone and the midlevel effects were due to the mesoscale circulations associated with the cloud bands (Fig. 2). It is of interest to note that although w'' was typically stronger at the midlevels above the sloping frontal zone where the cloud bands were formed (Szeto et al. 1999), the horizontal variability of the moisture field is relatively weak at these levels. On the other hand, the weaker w'' associated with the surface front was found in a region of strong horizontal thermal and moisture gradients (and hence the larger values of q''), resulting in the stronger vertical eddy moisture flux divergence at the lower levels (Fig. 5). These eddy moistening effects contributed to the differences between the large-scale moisture profiles of the fine-mesh and coarse-grid model systems shown in Fig. 4f. It should also be noted that although the absolute magnitudes of the moisture deficit in the coarse-grid cases are stronger at the low levels, the relative magnitudes of the differences are actually larger at the upper levels.

Some of the vertically transported moisture precipitated out but some of it would remain in the atmosphere, depending on the precipitation efficiency of the storm, which is typically somewhat less than unity for cyclonic systems (Szeto et al. 1997). When aggregated over many systems over the storm track, these differences in the

model storms would be revealed in the model climatology over the storm track regions. For example, the common underestimation of cloudiness and upper-level moisture over such regions in current large-scale models (Del Genio 1996; Stewart et al. 1998) might be attributed to these deficiencies of coarse-grid models in simulating synoptic cloud systems.

4. Conclusions

A winter oceanic cyclonic cloud system was simulated by using the MC2 model with different combinations of model resolution and cloud microphysics packages. The observed finescale storm structures in the warm-frontal region were replicated well in the high-resolution simulation. When aggregated to an area approximately equivalent to the size of a grid box in current GCMs, results from the simulations differ significantly in the large-scale cloud and moisture profiles. Although the effects of using different stratiform cloud schemes on the results are appreciable, the effects of different model resolution are shown to be greater on the large-scale frontal cloud field. In particular, the coarse-grid models underestimated the cloudiness and atmospheric moisture content in the warm-frontal region. Such differences in the large-scale model storm environment were consequences of the stronger mean cross-front circulation and mesoscale frontal cloud features in the high-resolution simulation. Because both the frontal zones and the mesoscale cloud bands are unresolved features in current GCMs, these results suggest that the parameterization of their bulk effects on the large scales must be included in the representation of frontal layered clouds in GCMs. Validated high-resolution model simulations that capture explicitly these finescale storm features should be very useful in the development of these parameterizations. In addition, the validated fine-mesh model results can be used in conjunction with the coarse-grid results to calibrate cloud schemes developed for mesoscale models so that they can be applied to GCMs. These model results also provide high-resolution synthetic datasets for deriving relationships relating the subgrid cloud properties and the large-scale variables. These relationships are needed for the parameterization of subgrid partial cloudiness and heterogeneous cloud effects in large-scale models. Studies are currently being carried out within the Global Energy and Water Cycle Experiment Cloud System Study Extratropical Layered Clouds working group to address some of these issues (see, e.g., Ryan et al. 2000; Szeto and Lohmann 1999).

Acknowledgments. The authors wish to thank Drs. Ronald E. Stewart and Jack Katzfey for insightful discussions and the anonymous reviewers for their useful comments and suggestions, which have considerably improved the manuscript.

REFERENCES

Benoit, R., M. Desgagne, P. Pellerin, S. Pellerin, and Y. Chartier, 1997: The Canadian MC2: A semi-Lagrangian, semi-implicit wideband atmospheric model suited for finescale process studies and simulation. *Mon. Wea. Rev.,* **125,** 2382–2415.

Del Genio, A. D., 1996: Observational requirements for modelling of global and regional climate change. *Remote Sensing of Processes Governing Energy and Water Cycles in the Climate System*, E. Raschke, Ed., NATO ASI Series, Vol. 45, Springer-Verlag, 31–57.

Houghton, J. T., L. G. Meiro Filho, B. A. Callander, N. Harris, A. Kattenburg, and K. Maskell, Eds., 1996: *Climate Change 1995: The Science of Climate Change.* Cambridge University Press, 572 pp.

Houze, R. A., and P. V. Hobbs, 1982: Organization and structure of precipitating cloud systems. *Advances in Geophysics*, Vol. 24. Academic Press, 225–315.

Hudak, D. R., R. E. Stewart, A. D. Thomson, and R. List, 1996: Warm frontal structure in association with a rapidly deepening extratropical cyclone. *Atmos.–Ocean,* **34,** 103–132.

Kong, F.-Y., and M. K. Yau, 1997: An explicit approach of microphysics in MC2. *Atmos.–Ocean,* **35,** 257–291.

Ryan, B. F., and Coauthors, 2000: Simulations of a cold front by cloud-resolving, limited-area, and large-scale models, and a model evaluation using in situ and satellite observations. *Mon. Wea. Rev.,* in press.

Stewart, R. E., K. K. Szeto, R. F. Reinking, S. A. Clough, and S. P. Ballard, 1998: Midlatitude cyclonic cloud systems and their features affecting large scales and climates. *Rev. Geophys.,* **36,** 245–273.

Sundqvist, H., E. Berge, and J. E. Kristjansson, 1989: Condensation and cloud parameterization studies with a mesoscale numerical weather prediction model. *Mon. Wea. Rev.,* **117,** 1641–1657.

Szeto, K. K., and U. Lohmann, 1999: Cloud-resolving and single-column model simulations of a synoptic cloud system: Implications for cloud parameterizations in GCMs. *Geophys. Res. Lett.,* **26,** 3113–3116.

——, R. E. Stewart, and J. M. Hanesiak, 1997: High latitude cold season frontal cloud systems and their precipitation efficiency. *Tellus,* **49A,** 439–454.

——, A. Tremblay, H. Guan, D. R. Hudak, R. E. Stewart, and Z. Cao, 1999: On the mesoscale dynamics of freezing rain storms over eastern Canada. *J. Atmos. Sci.,* **56,** 1261–1281.